Anal Bioanal Chem (2010) 398:867–876
DOI 10.1007/s00216-010-3964-5

ORIGINAL PAPER

Glucosamine-functionalized silver glyconanoparticles: characterization and antibacterial activity

Murugan Veerapandian · Suk Kyung Lim · Hyang Mi Nam · Gobianand Kuppannan · Kyusik S. Yun

Received: 28 April 2010 / Revised: 10 June 2010 / Accepted: 22 June 2010 / Published online: 11 July 2010

Abstract We report the analytical and in vitro antibacterial activity of glucosamine-functionalized silver glyconanoparticles. Morphological characterization ensured the surface topography and particle size distribution of both silver and glucosamine–silver nanoparticles. Surface plasmon resonance of both types of nanoparticle was determined from UV–visible spectroscopy using four different sample concentrations (10–40 μL). The resulting functionalized glyconanoparticles show maximum absorbance with a red shift of 30±5 nm (390–400 nm) from their initial absorbance (425–430 nm). FT-Raman and ^{1}H-NMR spectroscopic measurement confirmed the surface functionalization of glucosamine on the silver surface through the carbonyl group of a secondary amide linkage (–NH–CO–), elucidated by the conjugation of *N*-hydroxysuccinimide (NHS)-terminated silver nanoparticles and the amino group of glucosamine. Antimicrobial experiments with well-characterized silver nanoparticles (AgNPs) and glucosamine-functionalized silver nanoparticles (GlcN-AgNPs) demonstrate that GlcN-AgNPs have similar and enhanced minimum inhibitory concentration (MIC) against eight gram-negative and eight gram-positive bacteria compared with AgNPs. MIC data shows that *Klebsiella pneumoniae* (ATCC 700603) and *Bacillus cereus* isolate express high levels of inhibition, with the quantity and magnitude of inhibition being higher in the presence of GlcN-AgNPs.

Keywords Nanoparticle · Silver · Glucosamine · Glyconanoparticle · Antibacterial agent

Electronic supplementary material The online version of this article (doi:10.1007/s00216-010-3964-5) contains supplementary material, which is available to authorized users.

M. Veerapandian · K. S. Yun (✉)
College of Bionanotechnology, Kyungwon University, Gyeonggi-do 461-701, South Korea
e-mail: ykyusik@kyungwon.ac.kr

S. K. Lim · H. M. Nam
Bacteriology and Parasitology Division/Animal Disease Research Department, National Veterinary Research and Quarantine Service, Gyeonggi-do 430-824, South Korea

G. Kuppannan
Laboratory of Biomedicine, National Institute of Animal Sciences, Suwon 441-706, South Korea

Introduction

As bacteria resistant to commonly used antibiotics continue to increase in number, researchers are searching for new antibacterial agents. Development of drug resistance among bacteria is often because they acquire genes from other bacteria that have become resistant or because their genes mutate. Bacterial infection is far more serious and progresses quickly. For example, inflammatory diseases of the brain such as meningitis and encephalitis are among the top ten infectious causes of death [1] and result from bacteria such as *Bacillus anthracis*, *Bacillus subtilis*, or *Staphylococcus aureus* and fungi or viruses [2].

Silver nanoparticles (AgNPs) are some of the most alluring nanomaterials because of their unusual physiochemical and biological properties as well as their broad range of potential applications [3–5]. The versatile antimicrobial activity of silver has been well understood for centuries; however, interest in this transition metal has

recently been revived, particularly relating to its use against the increasing threat of antibiotic resistance resulting inter alias from abuse of several antibiotics [6, 7]. Ag is well known to inhibit bacterial growth and with a high safety margin. Silver is a relatively nontoxic natural inorganic metal and its nanoscale makes its total surface area larger in an identity volume [8]. Some studies have reported the biological activity of AgNPs and Ag-modified carbon nanotubes (CNT) [8], amphiphilic macromolecules [9], chitosan [10], silica nanospheres [11], and TiO_2 [12, 13], and these are reviewed elsewhere [14].

Glucosamine (GlcN) is also a naturally occurring amino sugar resulting from the amidation of fructose-6-phosphate [15]. A previous report suggested that glucosamine-mediated transglutaminase 2 (TGase 2) inhibition leads to nuclear factor kappa-light-chain-enhancer (NF-αB) activation in drug-resistant breast cancer cells, which evinced the promising role of GlcN as a TGase 2 inhibitor in the treatment of malignant cancer [16]. In addition, GlcN is a well known as an alternative cure in osteoarthritis.

Nanoparticles functionalized with sugar molecules as ligands are called glyconanoparticles. Silver nanoparticles functionalized with glucosamine provide a new class of glyconanoparticle [17]. Several varieties of glyconanoparticles such as gold and silver functionalized with tetrasaccharide [18], disaccharide [19], and monosaccharide [20] were reported. Some glyco-quantum dots and magnetic glyconanoparticles have also been studied [21, 22]. Applications of these glyconanoparticles include probes of carbohydrate–carbohydrate and carbohydrate–protein interactions, biolabels, antiadhesive therapy, bioamplification strategies, and in material science for microstructure manipulation, quantum dot and magnetic bioconjugation were studied [23]. Though there are enormous biomedical and material applications of the distinct glyconanoparticles, to the best of our knowledge there are no reports in the literature related to the antibacterial activity of the glyconanoparticles. We therefore screened our new class of glyconanoparticle, comprising metal silver and glucosamine as ligand [17], for antibacterial activity. A distinctive feature of the silver–glucosamine glyconanoparticles is their ability to form a homogeneous colloidal dispersion in water which is stable over a broad range of pH values.

The present study reports the structural and in vitro bacterial inhibition activity of glucosamine-functionalized silver nanoparticles (GlcN-AgNPs). The obtained results may help incorporate this additional feature (antibacterial activity) of glyconanoparticles in drug delivery and also provide a model system for particle-based sensor development and nanomedicine-based drug discovery.

Experimental

Materials

Silver nitrate ($AgNO_3$), D-(+)-glucosamine hydrochloride, and phosphate buffered saline (pH 7.4) (PBS) were obtained from Sigma. Sodium borohydride ($NaBH_4$), 11-mercaptoundecanoic acid (MUA), *N*-hydroxysuccinimide (NHS), and 1-ethyl-3-(3-dimethylaminopropyl)carbodiimide hydrochloride (EDC) were obtained from Aldrich. Milli-Q water with resistance 18 MΩ was used in all our experiments.

Synthesis of silver nanoparticles

Silver nanoparticles were synthesized by using an ultrasonic method modified from our previous report [24]. Aqueous solution of 2 mL of metal precursor $AgNO_3$ (30 mM) was added to the reaction vessel containing 4 mL of freshly prepared $NaBH_4$ (30 mM). A color change occurred almost immediately. (The reaction was repeated by using excess $NaBH_4$ but no change of intensity of absorption maximum occurred.) Then the reaction mixture was kept under ultrasonication using a Sonics VC505 for 45 min at a probe temperature of 80 °C, amplitude of 35%, and pulser on-off cycle 8–10s. The resulting colloidal solution was centrifuged, and the separated particles were washed twice with ethanol in an ultrasonication bath and dried in an oven at 80 °C for 4 h.

Synthesis of glucosamine-functionalized silver glyconanoparticles

Glucosamine was functionalized on silver nanoparticles in two steps (MUA modification and EDC/NHS coupling reaction) following the literature [17]. Briefly, 2.0 mL of colloidal AgNPs solution (approximately 0.8 nM) was gently added with 2.0 mL PBS (10 mM pH 7.4, with 0.2 mg/mL Tween-20) and the mixture was incubated with gentle shaking at 100 rpm for 30 min. Then 2.0 mL MUA solution (0.5 mM in 1:3 alcohol/H_2O) was added and the mixture was then gently shaken for 5 h to allow complete chemisorption of alkanethiol onto the AgNPs' surface. Then final mixture was centrifuged to remove excess alkanethiol and resuspended in PBS (with Tween-20). The resulting MUA-modified AgNPs were then reacted with the freshly prepared 50 mM NHS and 200 mM EDC solution for 1 h with stirring. The formed NHS-terminated AgNPs were centrifuged and redispersed in PBS (with Tween-20) under ultrasonication for the next wash. The washed NHS-terminated AgNPs were added dropwise to a flask containing 5 mL of 10 mM GlcN in PBS while stirring. Stirring was continued for another 3 h at

room temperature. The excess of GlcN was removed by centrifugation and redispersion of GlcN-AgNPs, which was repeated three times. Finally the GlcN-functionalized AgNPs were redispersed in PBS and stored at 4 °C.

Morphological characterization

Morphological information was obtained by using three different microscopes: a transmission electron microscope (TEM; Jeol-1010), atomic force microscope (AFM; Veeco Multimode V), and field emission scanning electron microscope (FE-SEM; Jeol-7500F). The prepared colloidal suspensions of AgNPs and GlcN-AgNPs were drop-coated and air-dried on a copper grid for TEM, freshly cleaved mica substrate for AFM, and platinum substrate for FE-SEM accordingly. In the case of FE-SEM imaging, the sample is air-dried and sputter-coated with platinum before examination in the electron microscope.

Analytical characterization

Specific UV–visible spectra were obtained at four different concentrations (10, 20, 30, and 40 μL in 100 μL ethanol) by using an Optizen 3220 in the range 300–600 nm. Fourier transform Raman spectroscopy was used to analyze the final AgNPs surface functionalized with GlcN (Bruker, Vertex 70). The laser beam was focused on the sample and the scattered light was collimated into the spectrometer by using a 180°-angle configuration. Raman spectra were collected at room temperature. Changes in the functional group of glucosamine after treatment on the AgNPs was obtained from NMR spectra (GlcN and GlcN-AgNPs) recorded by using a 400-MHz ^{1}H-NMR spectrometer (Bruker, Avance 400 WB; D_2O as solvent).

Antimicrobial study

Bacterial strains

Sixteen bacterial strains (eight gram-negative and eight gram-positive bacteria) were selected for the antibacterial activity test: gram-negative strains were *Escherichia coli* ATCC 25922, *E. coli* pig isolate, *Salmonella typhimurium* ATCC 14028, *S. typhimurium* pig isolate, *Salmonella enteritidis* ATCC 13076, *Pseudomonas aeruginosa* cattle isolate, *Klebsiella pneumoniae* ATCC 700603, and *K. pneumoniae* cattle isolate; gram-positive strains were methicillin-resistant *Staphylococcus aureus* human isolate, vancomycin-resistant *Enterococcus faecium* BM 4147, vancomycin-resistant *E. faecium* human isolate, *S. aureus* ATCC 29213, vancomycin-susceptible *E. faecium* ATCC 51558, *Bacillus subtilis* KCTC 3727, *B. subtilis* cattle isolate, and *Bacillus cereus* cattle isolate.

Antibacterial activity test

Antibacterial activity test was performed by agar dilution method [25] with twofold serial dilution of samples on Mueller–Hinton agar. Inocula were prepared by suspending growth from overnight cultures in sterile saline to a turbidity of a 0.5 McFarland standard. Final inocula contained 10^4 CFU/spot. Plates were inoculated with a Steers replicator with 3-mm inoculating pins and incubated for 16–20 h at 37 °C in aerobic conditions. The lowest concentration of antibiotic resulting in no growth was read as the minimum inhibitory concentration (MIC).

Results and discussion

Morphological characterization

Figure 1 shows the TEM (a, c) and FE-SEM (b, d) images of the AgNPs and GlcN-AgNPs. As observed in the electron micrographs, the AgNPs and GlcN-AgNPs are homogeneously dispersed in the aqueous solvent. Ultrasonochemically fabricated AgNPs are well distributed in the substrate. The acoustic microstreaming and cavitation force from the sonication probe creates the pressure waves which drastically minimize the ionic concentration gradient and enhance mass transport at the solid sphere–liquid interface [26], which results in the homogeneous synthesis of AgNPs. After GlcN functionalization a considerable modification occurs on the surface of the AgNPs, which is clearly evinced from the TEM and FE-SEM images. The average particle size distribution measurement from the TEM gave the size range of AgNPs as 20±2 nm and GlcN-AgNPs as 30±5 nm. As shown in Scheme 1, the GlcN functionalization occurred in the presence of PBS containing the nonionic surfactant Tween-20, which prevented the aggregation at high ionic strengths [27]. Figure 2 depicts the tapping mode AFM images of AgNPs and GlcN-AgNPs. AFM provides additional capabilities and advantages relative to other microscopic methods in studying the metallic surfaces and microstructures by providing reliable study at the nanometer scale [28]. Figure 2 shows the two different images of AgNPs and GlcN-AgNPs characterized by its phase (a and c) and 3D (b and d) view respectively. Structural information obtained from the AFM agreed well with the other two microscopic studies and, furthermore, confirmed the spherical structure of the AgNPs and GlcN-AgNPs.

UV–visible absorption spectroscopy

Among the metal nanoparticles, AgNPs are of particular interest owing to their third-order optical nonlinearity and pronounced surface plasmon resonance (SPR) absorption,

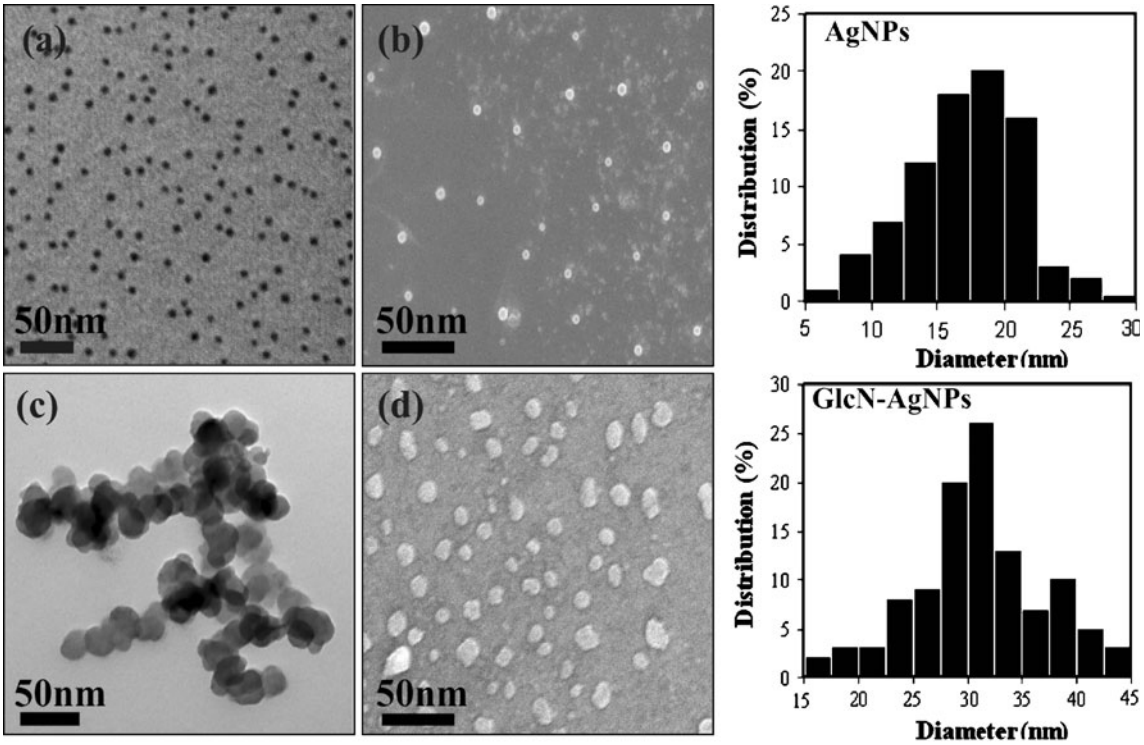

Fig. 1 TEM (*left*) and FE-SEM (*right*) images of AgNPs (**a**, **b**) and GlcN-AgNPs (**c**, **d**) and their corresponding average particle size distribution

which have promising roles in many applications, such as optical waveguides and optical switches [29]. The optical properties of the obtained AgNPs and GlcN-AgNPs were studied by using an Optizen 3220 spectrophotometer. Figure 3a and b shows the maximum absorbances of AgNPs and GlcN-AgNPs respectively. From Fig. 3a, the curve peak indicates the characteristic SPR of AgNPs between 390 and 400 nm (a–d = 10, 20, 30, and 40 μL in 100 μL ethanol) [30]. After surface functionalization of GlcN there are significant changes in the spectrum (Fig. 3b) distinguished by the broadened peak and shift of SPR to 425–430 nm (a–d = 10, 20, 30, and 40 μL in 100 μL ethanol). In general localized SPRs are obtained due to the collective oscillations of conductive electrons from the sample species. Appearance of strong SPR bands is generated from the excitation of localized surface plasmon resulting from the strong light scattering, by an electric field at a specific wavelength. The optical absorption spectrum of metal nanoparticles is dominated by the SPR, which leads to the distinguished red or blue shift depending on the dielectric properties of the surrounding host matrix, or the environmental atmosphere, in addition to the particle size and shape [31]. The SPR of GlcN-functionalized AgNPs is in the range 425–430 nm with a red shift of 30±5 nm relative to that of plain AgNPs. This is due to the introduction of the amino sugar GlcN on the AgNPs, which affects peak width thereby considerably increasing the metal surface coating. Subsequently surface modification leads to the confinement of the free electrons with the Ag metal, which strongly influenced the absorbance resulting in the red shift with a higher absorbance or reflection from its original intensity. As the concentration of the AgNPs and GlcN-AgNPs increases from 10 to 40 μL in the analysis, the absorbance radiant energy increased coherently along with the extinction coefficient. This result also highlights the stability of AgNPs and GlcN-AgNPs in the solvent ethanol.

FT-Raman spectroscopy

In order to confirm the successful functionalization of GlcN on the AgNPs surface structurally, FT-Raman spectroscopy was used to obtain the conformational bands of GlcN. Figure 4 shows the characteristic Raman bands observed for the final GlcN-AgNPs over the range 500–3,500 cm^{-1}. The distinct stretching and bending vibrations from the GlcN-AgNPs structure containing carbon-linked hydroxyl, CH, and primary amine conjugated groups are well resolved as follows. From Fig. 4, the sharp band observed at 876 cm^{-1} is assigned to be C(1)-H. The shift observed at 1,042–1,081 cm^{-1} and a moderate peak at 1,702 cm^{-1} were attributed to the C–O functional moiety of GlcN. A strong, intense Raman peak at 1,451 cm^{-1} relates to the CH and C (6)-OH vibrations. The weak band located at 1,270 cm^{-1} is due to the C–OH group. In a previous study, laser Raman spectra of plain D-glucosamine hydrochloride were reported

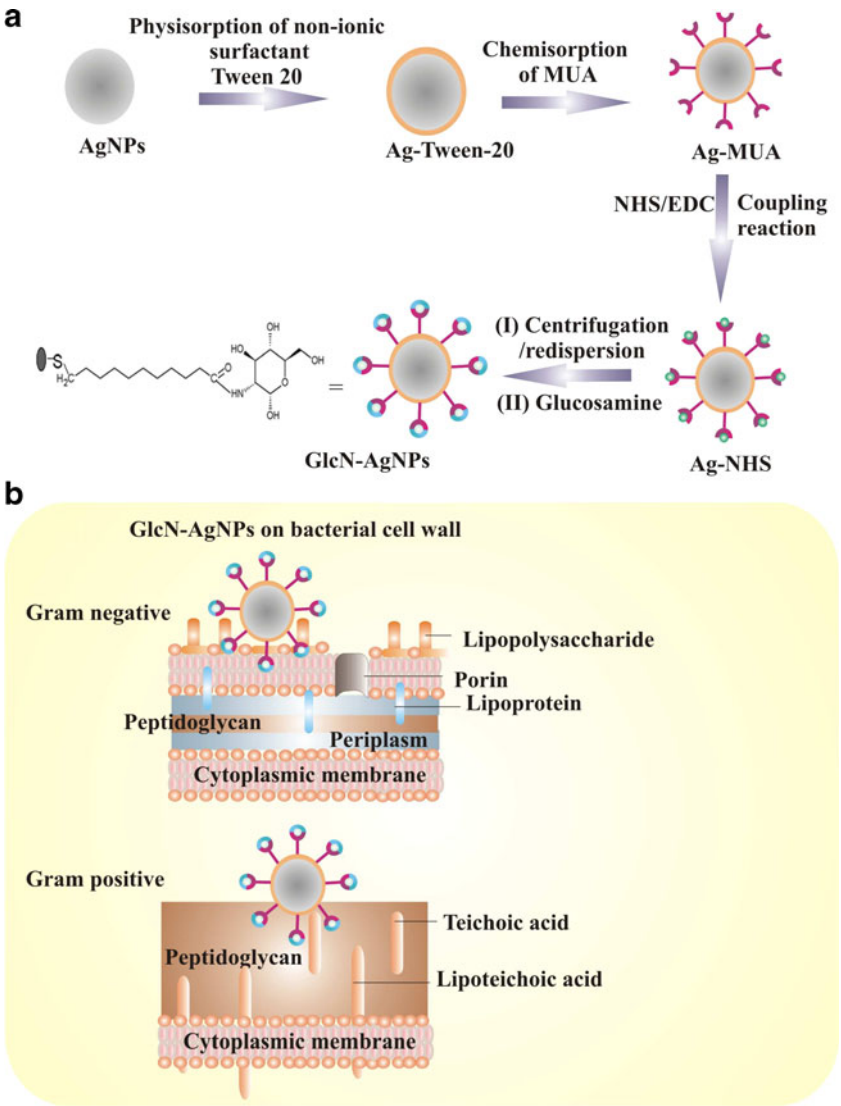

Scheme 1 Functionalization of glucosamine on silver nanoparticles (**a**) and the interaction of GlcN-AgNPs with bacterial cell wall surface (**b**)

to have distinct vibrations at 1,520, 1,583, and at 1,620 cm^{-1}, which were assigned to NH_3^+ [32]. In our case, the carbonyl group of the secondary amide (–CO–NH–) linkage obtained by the conjugation of NHS-terminated AgNPs and the amino group of GlcN was observed at 1,574 cm^{-1} and 1,663 cm^{-1}. The significant CH stretches from CH_2 groups present on the surface of the Ag colloid and in GlcN after functionalization were resolved at 2,720 (CH), 2,882 (C(6)-H), 2,932, and 2,974 cm^{-1} (C(2)-H) respectively. The vibration for hydroxyl groups of GlcN displays a broad stretching at 3,221 and 3,329 cm^{-1}.

^{1}H-NMR spectroscopy

To understand the chemical modification in more depth, a ^{1}H-NMR spectral analysis was performed on the final GlcN-AgNPs (Fig. 5). Their characteristic resonances corresponding to different units of the GlcN-functionalized AgNPs are discussed as follows. A singlet peak centered at δ_H 7.27 was attributed to the –N*H*–CO– of the secondary amide linkage [17, 33]. The multiplet at δ_H 4.51–4.05 corresponds the –C*H*- proton from the Ag surface colloid. The weak signal near δ_H 3.88 and a triplet peak centered at δ_H 3.80 were due to the –O*H* protons of GlcN. The multiplet signal at δ_H 2.38 and a signal at δ_H 2.36–2.29 relate the –C*H*– of GlcN. Resonance shift at δ_H 1.69–1.40 and a very weak triplet signal centered at δ_H 1.39 were assigned to the sp^3-hybridized –C*H*– proton from GlcN [17]. The successful functionalization of GlcN on the Ag surface was identified from the formation of the secondary amide linkage (–N*H*–CO–) resulting in a specific resonance located at δ_H 7.2 ppm (^{1}H-NMR) and stretching at 1,574 and 1,663 cm^{-1} (FT-Raman).

Antimicrobial study

The pharmacological action of silver against bacterial strains is generally reported to involve the interaction of

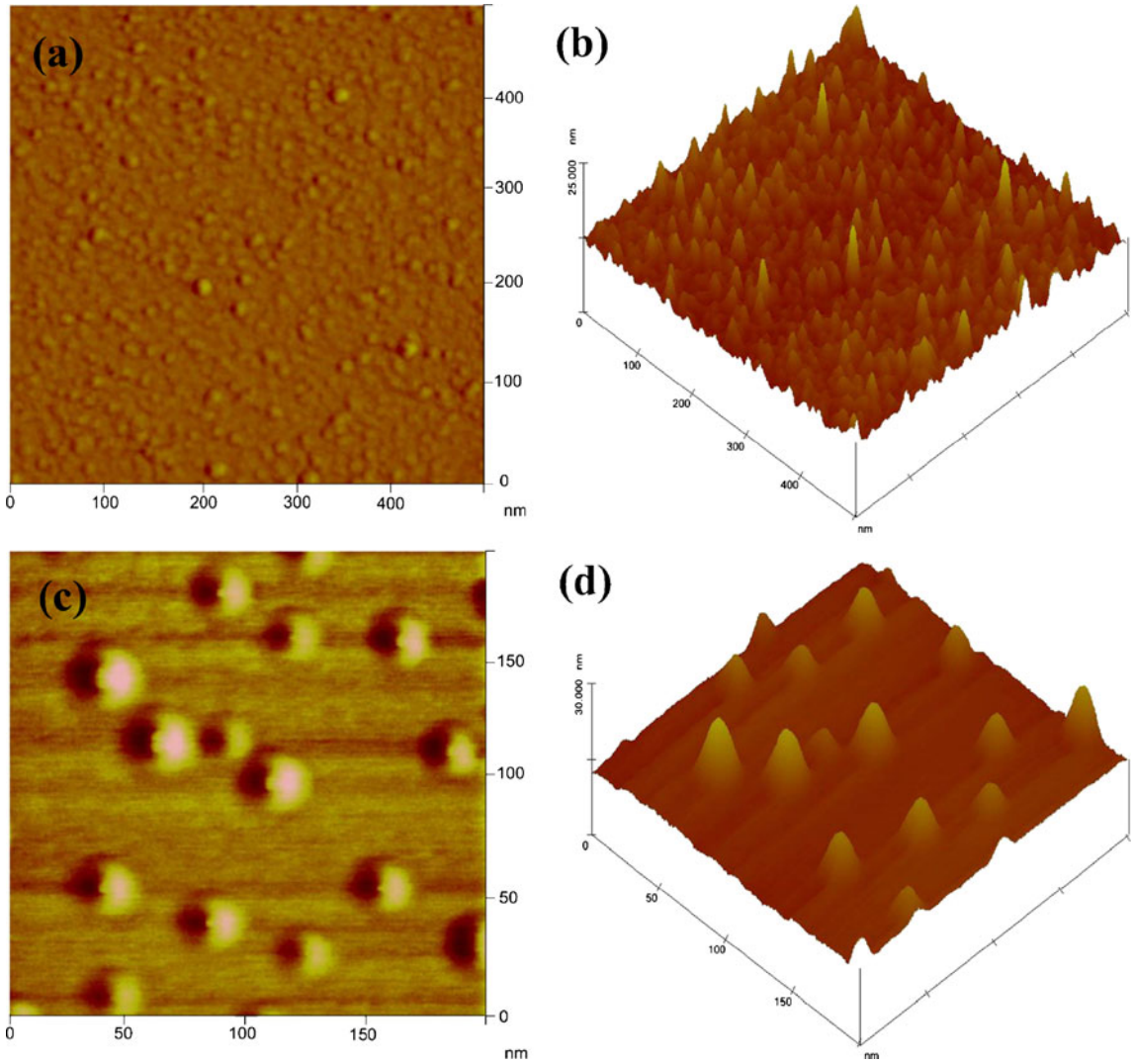

Fig. 2 Tapping mode AFM images of AgNPs (**a**; phase and **b**; 3D) and GlcN-AgNPs (**c**; phase and **d**; 3D) respectively

silver ions with disulfide or sulfhydryl groups of enzymes, causing physiological changes that lead to disruption of metabolic processes followed by cell death [34, 35]. The inhibitory action of AgNPs is also based on the release of Ag^+ ion [36]. Exposure of microorganisms to AgNPs was shown to result in strong antimicrobial activity [37, 38]. In addition to the increased surface area and associated increased potential for the release of Ag^+ ions, when dispersed in liquid suspensions, AgNPs may accumulate in the bacterial cytoplasmic membrane, causing a significant increase in permeability and cell death [39] by penetrating the bacterial cells [40]. In another report the antimicrobial mechanism of AgNPs was elucidated to involve the generation of free radicals from the surface of the nanoparticles, causing damage to the cellular membrane [14]. The bactericidal effect of nanoparticles is also dependent on the concentration of nanoparticles and the initial bacterial concentration [41].

In this study we comparatively evaluated the antibacterial activity of the silver and silver-functionalized glucosamine glyconanoparticles based on MICs of dispersed nanoparticles in batch cultures. Agar dilution method [25] was utilized to study the growth profile of a variety of bacterial species at various concentrations. Undiluted AgNPs were used as the control drug for this MIC screening. Representative images of bacterial growth inhibition in the presence of AgNPs and GlcN-AgNPs of varying concentrations are depicted in the "Electronic supplementary material" (Fig. S1). As the concentration of nanoparticles increased to the MIC of the respective strains, no growth was observed in the petri plate. Among the two *E. coli* strains selected for the study the strain most sensitive to AgNPs and GlcN-AgNPs was ATCC 25922. MICs observed for that strain were 8 μg/mL (AgNPs) and 4 μg/mL (GlcN-AgNPs), which are lower than the MIC of AgNPs for *E. coli* reported in previous studies conducted

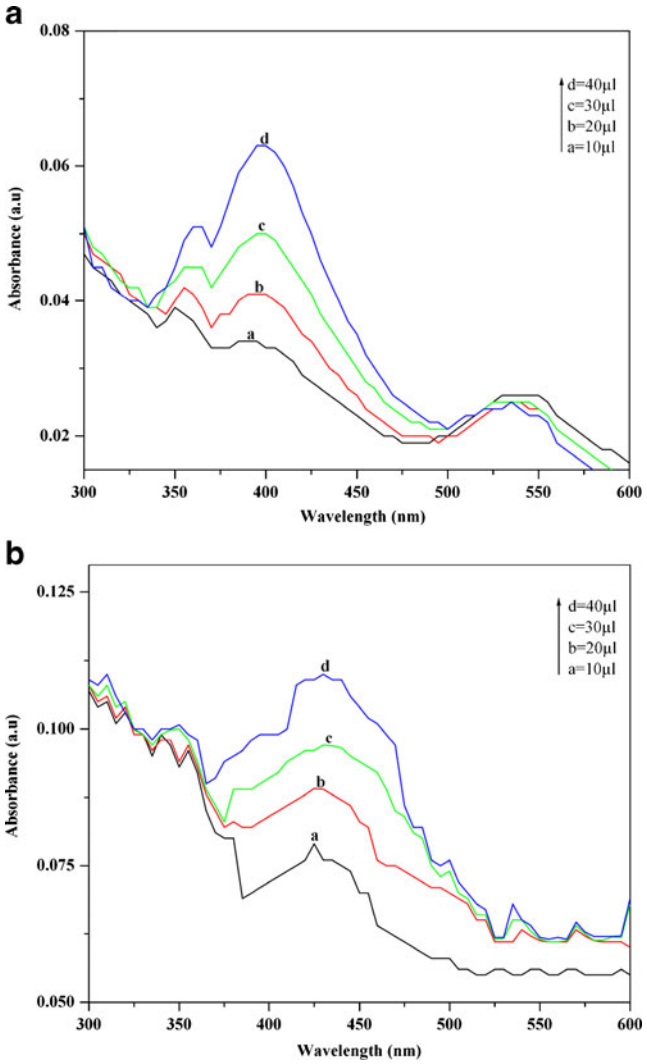

Fig. 3 UV–visible absorption spectrum of **a** AgNPs and **b** GlcN-AgNPs

on agar plates (75 µg/mL) [38]. In batch studies with *E. coli* and colloidal AgNPs (size range 2–25 nm), MIC was reported to be in the range of 3–25 µg/mL for initial bacterial concentration of 10^5–10^8 CFU/mL [42–44]. The MICs of AgNPs and GlcN-AgNPs on pig isolated *E. coli* strain were higher compared to the standard strain and were 512 µg/mL and 256 µg/mL respectively. MICs of the AgNPs and GlcN-AgNPs against the *S. typhimurium* ATCC 14028 and its pig isolate were 16 and 512 µg/mL. It is reported that Ag, Cu and chitosan-coated Ag, Cu nanoparticles have pronounced antibacterial activity against *S. typhimurium* [45]. In our study, GlcN-functionalized AgNPs had similar MIC values to AgNPs against *S. typhimurium* ATCC 14028 (16 µg/mL) and *S. typhimurium* pig isolate (512 µg/mL). Among the gram-negative bacterial strains *S. typhimurium* (pig isolate), *S. enteritidis* ATCC 13076, and *P. aeruginosa* (cattle isolate) had the least sensitivity towards the AgNPs and GlcN-AgNPs. But notably, the MIC of GlcN-AgNPs against *P. aeruginosa* was 256 µg/mL. Compared with the standard *E. coli* (ATCC 25900) strain, the standard *K. pneumoniae* (ATCC 700603) and cattle isolated *K. pneumoniae* strain were highly sensitive to AgNPs (MIC16 and 8 µg/mL) and GlcN-AgNPs (MIC 8 µg/mL). Antibacterial activities of AgNPs and GlcN-AgNPs against gram-positive bacteria were investigated by using eight strains. In general, gram-positive bacteria appeared to be more tolerant to silver than gram-negative cells. It has previously been reported that gram-positive bacteria are less susceptible to the antimicrobial activity of silver [14, 46]. It was emphasized that this may be due to differences in the cell wall physiology. The cell wall of gram-positive bacteria contains complex layers of peptidoglycan compared with the cell wall of gram-negative bacteria. Peptidoglycan is a complex structure and often contains teichoic acids or lipoteichoic acids which have a strong negative charge, which may contribute to sequestration of free Ag^+ ions. Thus, gram-positive bacteria may allow less Ag^+ to reach the cytoplasmic membrane than gram-negative bacteria and may therefore be less susceptible [45]. However in the present study, the MICs of AgNPs and GlcN-AgNPs were not significantly different between gram-negative and gram-positive strains. This may be due to the common resistance development among the bacterial species. Scheme 1B illustrates the process of interaction between the GlcN-AgNPs and bacterial cell wall distinguished by gram-negative and gram-positive bacteria. One study reported that AgNPs biosynthesized from *S. aureus* have antimicrobial activity against methicillin-resistant *S. aureus* (MRSA) and methicillin-resistant *S. epidermidis* (MRSE) [46]. The antibiotic activity of those bionanoparticles (determined using 0.002 mg of the AgNPs as the final product for the antimicrobial assay by zone of

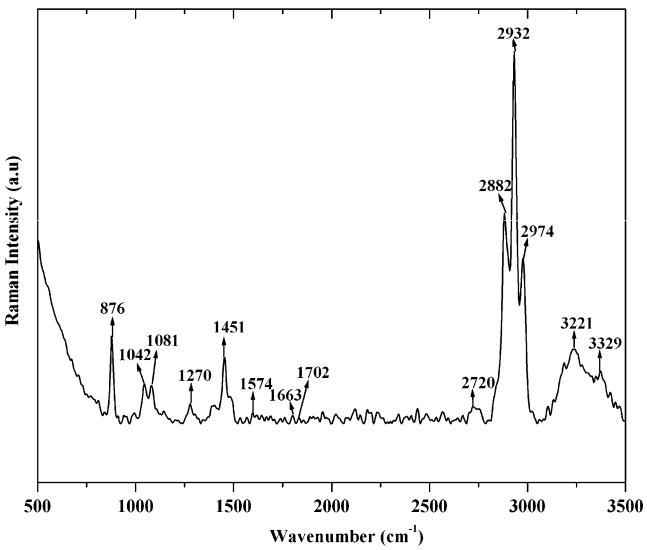

Fig. 4 FT-Raman spectrum of GlcN-AgNPs

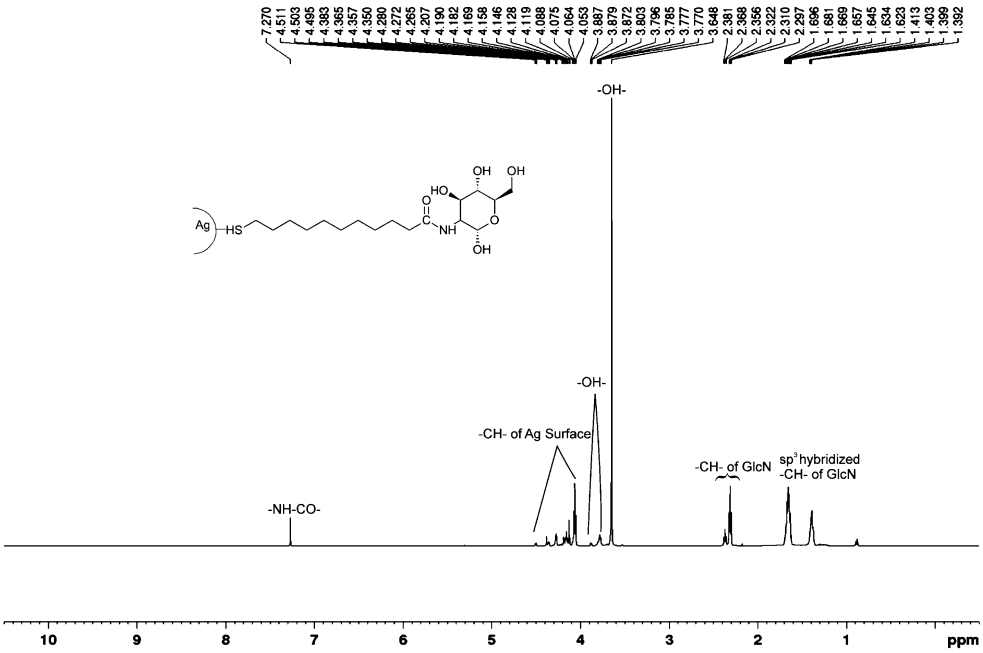

Fig. 5 ^{1}H-NMR spectrum of GlcN-AgNPs

inhibition) for MRSE (18 mm) and MRSA (17.5 mm) made the revival of the use of silver as a powerful bactericide possible. In another study some sulfonamide derivatives were reported to have MICs of 32, 64, and 128 μg/mL in different clinical isolates and showed promise against staphylococci infections, especially urinary infections [47]. For the better evaluation in our study, we chose human isolated MRSA and methicillin-sensitive *S. aureus* (ATCC 29213). The resulting MICs of AgNPs (16 and 128 μg/mL) and GlcN-AgNPs (8 and 128 μg/mL) against human isolate MRSA and methicillin-sensitive *S. aureus* provide evidence that these NPs are a promising nanomedicine against these pathogenic strains. AgNPs and GlcN-AgNPs have similar MICs against the vancomycin-resistant *E. faecium* (human isolate and standard) and the sensitive strain were found to be 256, 512, and 512 μg/mL respectively. Finally the MICs of AgNPs against the *B. subtilis* (KCTC 3727 and cattle isolate) and *B. cereus* (cattle isolate) were determined to be 256, 8, and 4 μg/mL, whereas GlcN-AgNPs had higher inhibition values compared with AgNPs on cattle isolated *B. subtilis* and *B. cereus*, found to be 4 and 2 μg/mL. MIC values of AgNPs and GlcN-AgNPs against the individual strains are shown in Table 1. It is worth noting that there is a significant batch-to-batch diversity, for instance, in the same species of *E. coli, S. typhimurium*, and *S. aureus*. This could be due to the variations in the physiochemical and biological properties of the nanoparticles. Furthermore, the selection of strains (isolates and commercial) plays a vital

Table 1 Minimum inhibitory concentration (MIC) of AgNPs and GlcN-AgNPs against eight gram-negative and eight gram-positive bacterial strains

Bacterial strains	AgNPs MIC (μg/mL)	GlcN-AgNPs MIC (μg/mL)
Gram-negative strains		
E. coli ATCC 25922	8	4
E. coli isolate	512	256
S. typhimurium ATCC 14028	16	16
S. typhimurium isolate	512	512
S. enteritidis ATCC 13076	512	512
P. aeruginosa isolate	512	256
K. pneumoniae ATCC 700603	16	8
K. pneumoniae isolate	8	8
Gram-positive strains		
S. aureus ATCC 29213 (MET^{s})	128	128
S. aureus isolate (MET^{r})	16	8
E. faecium ATCC 51558 (VAN^{s})	512	512
E. faecium BM 4147 (VAN^{r})	256	256
E. faecium isolate (VAN^{r})	512	512
B. subtilis KCTC 3727	256	256
B. subtilis isolate	8	4
B. cereus isolate	4	2
Control[a]	>512	>512

MET^{s} methicillin susceptible, MET^{r} methicillin resistant, VAN^{s} vancomycin susceptible, VAN^{r} vancomycin resistant

[a] Undiluted drug AgNPs

role in their different pharmacological actions and resistance development. The commercially available strains showed higher inhibition than isolates utilized for the MIC tests. The MIC values against the isolates agreed well with those reported for drugs like sulfonamide derivatives [47]. The similar or enhanced inhibition with minimum concentration of GlcN-functionalized AgNPs compared with only AgNPs in all strains could possibly due to the underlying structure–activity relationship of glucosamine, which is similar to chitosan except that glucosamine is a single monomer, whereas chitosan is a linear polysaccharide composed of randomly distributed β-(1–4)-linked D-glucosamine (deacetylated unit) and *N*-acetyl-D-glucosamine (acetylated unit). However in our compound the primary amino group of glucosamine reacted with the silver surface functionalized with NHS during the coupling reaction. The functionalization on the primary amino group converted it into the secondary amide, for which a relationship between chemical structure and antimicrobial activity has been reported [48]. In mammalian systems, increased glycolytic flux stimulates production of glucosamine-6-phosphate (GlcN-6-P) through the hexosamine biosynthetic pathway. Activation of this pathway by high glucose levels has been linked to insulin resistance in mammalian cells [49, 50]. It has been suggested that exogenous glucosamine (GlcN) exerts anti-inflammatory effects by inhibiting neutrophil functions such as the generation of superoxide and the release of granule enzymes [51]. Increased hexosamine flux can lead to increased O-linked glycosylation of proteins and inhibition of the oxidative pentosephosphate (OPP) pathway, either or both of which can potentially mediate the physiological effects of GlcN in mammalian cells. These reports gave evidence of the ability of GlcN to produce oxidative stress. Collectively dissolution and release of Ag^+ are reported to inhibit respiratory enzymes, reactive oxygen species (ROS) production, and disruption of membrane integrity and transport processes [52, 53]. However further investigations like gene expression of oxidative stress on bacterial cells are required to prove the mechanism of ROS production from GlcN-AgNPs.

Conclusion

The results of the present study allowed us to define a schematic approach for analytical and biological characterization of silver and glucosamine-functionalized silver nanoparticles. Morphological characterization revealed the particle size distribution range of 20±2 nm (AgNPs) and 30± 5 nm (GlcN-AgNPs). UV–visible spectra evinced the surface modification of GlcN on the Ag surface. ^{1}H-NMR and FT-Raman spectroscopy allowed the structural elucidation of the functionalized glyconanoparticles through appearance of the characteristic –NH–CO resonance at δ_H 7.29 ppm and Raman band at 1,574 and 1,663 cm^{-1} respectively. This new class of glyconanoparticle exhibits pronounced in vitro antibacterial activity against eight gram-negative and gram-positive bacteria in a concentration-dependent manner. The enhanced antibacterial activity of GlcN-Ag glyconanoparticles may be attributed to: (1) surface functionalization with an amino sugar (glucosamine), which facilitates the distribution and penetration of glyconanoparticles into the bacterial cell surface; (2) a larger surface area for contact and interaction with the cell surface; and/or (3) unique structure–activity relationship. Furthermore, the properties of the glyconanoparticles make them attractive as a hydrophilic, biodegradable, and stable nanomaterial for a wide range of biomedical applications including antimicrobial nanomedicine, sensors, and as a model system for studies of several biointeractions such as carbohydrate–protein, carbohydrate–carbohydrate, and carbohydrate–cell.

Acknowledgements This work was supported by Kyungwon University research fund in 2010. This work was also supported by GRRC program of Gyeonggi province [2009-B02, Development of biodevice using DNA tile structure].

References

1. Obermaier B, Klein M, Koedel U, Pfister HW (2006) Drug Discov Today 3:105–112
2. Ewald C, Kuhn S, Kalff R (2006) Neurosurg Rev 29:163–167
3. Li Z, Lee D, Sheng XX, Cohen RE, Rubner MF (2006) Langmuir 22:9820–9823
4. Chen YY, Wang C, Liu HY, Qiu JS, Bao XH (2005) Chem Commun 42:5298–5300
5. Setua P, Chakraborty A, Seth D, Bhatta MU, Satyam PV, Sarkar N (2007) J Phys Chem C 111:3901–3907
6. Sambhy V, MacBride MM, Peterson BR, Sen A (2006) J Am Chem Soc 128:9798–9808
7. Panaek A, Kvitek L, Prucek R, Kola M, Veeova R, Pizurova N, Sharma VK, Nevena T, Zboril R (2006) J Phys Chem B 110:16248–16253
8. Vijaya KR, Ghouse MM, Shaik J, Angel H, Komal V, Shree RS, Shreekumar P (2010) Nanotechnology 21:095102.1–095102.11
9. Aymonier C, Schlotterbeck U, Antonietti L, Zacharias P, Thomann R, Tiller JC, Mecking S (2002) Chem Commun 24: 3018–3019
10. Dongwei W, Wuyong S, Weiping Q, Yongzhong Y, Xiaoyuan M (2009) Carbohydr Res 344:2375–2382
11. Jie-Xin W, Li-Xiong W, Zhi-Hui W, Jian-Feng C (2006) Mater Chem Phys 96:90–97
12. Sökmen M, Değerli S, Aslan A (2008) Exp Parasitol 19(1):44–48
13. Zheng J, Hua Y, Xinjun L, Shanqing Z (2008) Appl Surf Sci 254 (6):1630–1635
14. Kim J, Kuk E, Yu K, Kim J, Park S, Lee H, Kim S, Park Y, Park Y, Hwang C (2007) Nanomedicine 3:95–101
15. Ju HW, Koh EJ, Kim SH, Kim KI, Lee H, Hong SW (2009) J Plant Physiol 166:203–212
16. Kim DS, Park KS, Jeong KC, Lee BI, Lee CH, Kim SY (2009) Cancer Lett 273:243–249

17. Veerapandian M, Yun KS (2010) Synth React Inorg Met-Org Nano-Met Chem 40(1):56–64
18. De Paz JL, Ojeda R, Barrientos AG, Penadés S, Martín-Lomas M (2005) Tetrahedron Asymmetry 16:149–158
19. De la Fuente JM, Barrientos AG, Rojas TC, Rojo J, Cañada J, Fernández A, Penadés S (2001) Angew Chem Int Ed 40:2257–2261
20. Barrientos AG, De la Fuente JM, Rojas TC, Fernández A, Penadés S (2003) Chem Eur J 9:1909–1921
21. De la Fuente JM, Penadés S (2005) Tetrahedron Asymmetry 16:387–391
22. Penades S, Martin-Lomas M, De la Fuente JM, Rademacher TW (2004) Magnetic nanoparticles. WO Patent 2004/108165 A2
23. De la Fuente JM, Penadés S (2006) Biochim Biophys Acta 1760:636–651
24. Veerapandian M, Yun KS (2010) Ultrasonochemical-assisted fabrication and evaporation-induced self-assembly (EISA) of POSS-SiO_2@Ag core/ABA triblock copolymer nanocomposite film. Polym Compos. doi:10.1002/pc.20951
25. Wickler MA et al (2009) Methods for dilution antimicrobial susceptibility testing for bacteria that grow aerobically. Clinical Laboratory and Standards Institute, Wayne, Pennsylvania
26. Awati PS, Awate SW, Shah PP, Ramaswamy V (2003) Catal Commun 4:393–400
27. Aslan K, Prez-Luna VH (2002) Langmuir 18(16):6059–6065
28. Goeken M, Kempf M (1999) Acta Mater 47:1043–1052
29. Maruyama O, Senda Y, Omi S (1999) J Non-Cryst Solids 259:100–106
30. Chen W, Zhang J, Shi L, Di Y, Fang Q, Cai W (2003) Compos Sci Technol 63:1209–1212
31. Von Fragstein C, Schoenes FJZ (1967) Z Phys 198:477
32. She CY, Dinh ND, Anthony TT (1974) Biochim Biophys Acta 372:345–357
33. Oya M, Negishi T (1984) Bull Chem Soc Jpn 57:439–441
34. Butkus MA, Edling L, Labare MP (2003) J Water Supply Res Technol AQUA 52:407–416
35. Feng QL, Wu J, Chen GQ, Cui FZ, Kim TN, Kim JO (2000) J Biomed Mater Res 52:662–668
36. Morones JR, Elechiguerra JL, Camacho A, Holt K, Kouri JB, Ramirez JT, Yacaman MJ (2005) Nanotechnology 16:2346–2353
37. Baker C, Pradhan A, Pakstis L, Pochan DJ, Ismat Shah S (2005) J Nanosci Nanotechnol 5:244–249
38. Cho KH, Park JE, Osaka T, Park SG (2005) Electrochim Acta 51:956–960
39. Sondi I, Salopek-Sondi B (2004) J Colloid Interface Sci 275:177–182
40. Raffi M, Hussain F, Bhatti TM, Akhter JI, Hameed A, Hasan MM (2008) J Mater Sci Technol 24:192–196
41. Pal S, Tak, Song JM (2007) Appl Environ Microbiol 73:1712–1720
42. Aleš P, Libor K, Robert P, Milan K, Renata V, Naděžda P, Virender KS, Tatĵana N, Radek Z (2006) J Phys Chem B 110:16248–16253
43. Gogoi SK, Gopinath P, Paul A, Ramesh A, Ghosh SS, Chattopadhyay A (2006) Langmuir 22:9322–9328
44. Uparelia JP, Chatterjee AK, Duttagupta SP, Mukherji S (2008) Acta Biomater 4:707–716
45. Kawahara K, Tsuruda K, Morishita M, Uchida M (2000) Dent Mater 16:452–455
46. Nanda A, Saravanan M (2009) Nanomedicine 5:452–456
47. Yeliz G, Resịt Ö, Yunus B (2008) Ann Clin Microbiol Antimicrob 7(17):1–6
48. Jon JK, Anthony JC, Joseph PT (1972) Antimicrob Agents Chemother 2(6):492–498
49. Marshall S, Bacote V, Traxinger RR (1991) J Biol Chem 266:4706–4712
50. McClain DA (2002) J Diabetes Complicat 16:72–80
51. Hua J, Sakamoto K, Nagaoka I (2002) J Leukoc Biol 71:632–640
52. Hussain SM, Hess KL, Gearhart JM, Geiss KT, Schlager JJ (2005) Toxicol In Vitro 19:975–983
53. Navarro E, Baun A, Behra R, Hartmann NB, Filser J, Miao AJ, Quigg A, Santschi PH, Sigg L (2008) Ecotoxicology 17:372–386